ACS Medicinal Chemistry Letters

pubs.acs.org/acsmedchemlett Letter

Discovery of Potent Inhibitors of *Streptococcus mutans* Biofilm with Antivirulence Activity

Bhavitavya Nijampatnam,[⊥] Parmanand Ahirwar,[⊥] Piyasuda Pukkanasut, Holly Womack, Luke Casals, Hua Zhang, Xia Cai, Suzanne M. Michalek, Hui Wu,* and Sadanandan E. Velu*

Cite This: *ACS Med. Chem. Lett.* 2021, 12, 48−55

Read Online

ABSTRACT: Dental caries is a bacterial infectious disease characterized by demineralization of the tooth enamel. Treatment of this disease with conventional antibiotics is largely ineffective as the cariogenic bacteria form tenacious biofilms that are resistant to such treatments. The main etiological agent for dental caries is the bacterium *Streptococcus mutans*. *S. mutans* readily forms biofilms on the tooth surface and rapidly produces lactic acid from dietary sucrose. Glucosyl transferases (Gtfs) secreted by *S. mutans* are mainly responsible for the production of exopolysaccharides that are crucial for the biofilm architecture. Thus, inhibiting *S. mutans'* Gtfs is an effective approach to develop selective biofilm inhibitors that do not affect the growth of oral commensals. Herein, we report a library of 90 analogs of the previously identified lead compound, **G43**, and exploration of its structure activity relationships (SAR). All compounds were evaluated for the inhibition of *S. mutans* biofilms and bacterial growth. Selected compounds from this library were further evaluated for enzyme inhibition against Gtfs using a zymogram assay and for growth inhibition against oral commensal bacterial species such as *Streptococcus gordonii* and *Streptococcus sanguinis*. This study has led to the discovery of several new biofilm inhibitors with enhanced potency and selectivity. One of the leads, $\mathbf{III_{F1}}$, showed marked reduction in buccal, sulcal, and proximal caries scores in a rat model of dental caries.

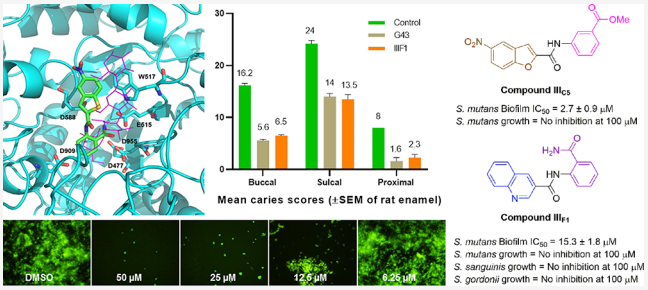

KEYWORDS: *Dental caries, Streptococcus mutans, biofilm, glucosyl transferases, SAR, in vivo*

Dental caries is considered to be a major health concern worldwide.[1] *Streptococcus mutans (S. mutans)* is the main etiological agent of dental caries.[2,3] In addition to its ability to adhere to tooth and form biofilm, *S. mutans'* potential to initiate dental caries also stems from its ability to create and thrive in an acidic oral microenvironment.[4−6] Through the function of its glucosyl transferases (Gtfs), namely GtfB, GtfC, and GtfD, *S. mutans* metabolizes dietary sucrose into water-insoluble and soluble glucans.[7] GtfB synthesizes water-insoluble glucans and GtfC synthesizes both water-insoluble and soluble glucans, whereas GtfD synthesizes only water-soluble glucans.[8,9] These exopolymeric glucans play an important role in mediating the irreversible attachment of *S. mutans* to the tooth surface. Glucans also serve as an extracellular matrix, shielding the bacteria from the host's immune responses, mechanical stress, and antimicrobial agents.[10]

There are several approaches available for the treatment of dental caries such as the use of fluoride in toothpaste and the use of antimicrobial mouthwashes. The removal of bacteria by brushing demands frequent repetition due to the rapid recolonization of tooth surfaces. Mouthwashes lack selectivity affecting both pathogenic and commensal species alike.[11] Recent studies have suggested that the use of such mouthwashes can increase blood pressure due to the damage caused to oral microbiota that have the aptitude to relax blood vessels.[12] In addition, a significant correlation exists between poor oral health and an increased risk for cardiovascular diseases.[13] Thus, there is an unmet need to develop innovative approaches to combat the persistent pathogenic oral biofilms. In order to preserve the natural oral bacterial flora, we sought to develop nonbactericidal agents that can selectively inhibit the cariogenic biofilms.

Several previous studies have validated Gtfs as potential targets for the development of therapeutic agents that can selectively inhibit cariogenic biofilms.[14,15] Mutants defective in genes coding for GtfB and GtfC cause markedly reduced levels of smooth surface caries lesions as compared to parental *S. mutans*.[16] Polyphenols[17−20] that include catechins, flavonoids, proanthocyanidin oligomers, and other plant-derived analogs[21] and synthetic small molecules[22] have been found to display

Received: July 7, 2020
Accepted: November 25, 2020
Published: December 7, 2020

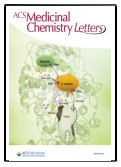

modest antibiofilm activities by modulating the expression or the activity of Gtfs. However, the selectivity of these compounds for biofilm inhibition opposed to growth inhibition remains to be determined, and their biofilm inhibitory potencies are low.

We have recently reported a novel Gtf inhibitor **G43** (Figure 1A) identified by *in-silico* screening using the reported GtfC X-ray crystal structure as target.[23] **G43** inhibited *S. mutans* biofilm in a dose dependent manner with an IC_{50} value of 16.7 μM, but it did not inhibit the growth of *S. mutans* or other oral commensal species up to 200 μM, indicating that it is a selective biofilm inhibitor (Figure 1B).[23] We have now completed the SAR studies on **G43** by generating a library of 90 analogs in order to optimize its activity and to identify additional derivatives that are suitable for preclinical development.

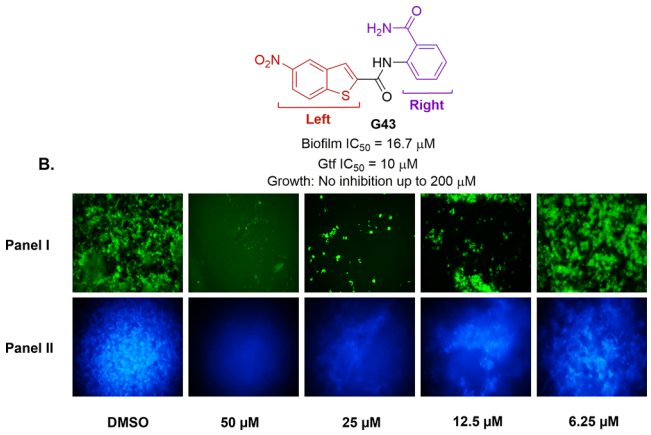

Figure 1. (A) Chemical structure of **G43**. (B) Fluorescent microscopy images of *S. mutans* UA159 biofilms with **G43** treatment using serial dilutions. Panel I: Viable bacterial cells within the biofilm were stained with 2.5 μM Syto9 (green). Panel II: Dextran-conjugated cascade blue labeled exopolysaccharides within *S. mutans* biofilms.

We designed this library starting from a series of carboxylic acids ($\mathbf{I_{A\text{-}J}}$) and the amine derivatives ($\mathbf{II_{1\text{-}9}}$) as shown in Figure 2. The left side modifications (R_1) included 5-nitroindole, 5-methoxyindole, 5-nitrobenzofuran, 3-quinolyl, 2-quinolyl, α-naphthyl, β-naphthyl, the 4-biphenyl group, and the right side modifications (R_2) included the $-CONH_2$ and $-COOMe$ groups at 2-, 3-, and 4- positions and a $-CH_2NH_2$ group at the 2-position of the phenyl ring and an unsubstituted phenyl ring. This library was synthesized in one step by an established amide coupling reaction using *N*-ethyl-*N*′-(3-(dimethylamino)propyl)carbodiimide (EDC) and *N*,*N*-dimethyl aminopyridine (DMAP) in dichloromethane (CH_2Cl_2). This procedure is amenable for the solution phase parallel synthesis as it takes place under mild conditions and the byproducts are removable by aqueous workup. It produced the expected amide products ($\mathbf{III_{A1\text{-}J8}}$) in yields ranging from 26 to 99% (Table 1). The Boc protecting group present in compounds $\mathbf{III_{A8\text{-}J8}}$ was removed by treatment with trifluoroacetic acid (TFA) to generate the aminomethyl derivatives $\mathbf{III_{A9\text{-}J9}}$. Out of the 90 library compounds, 15 indole derivatives ($\mathbf{III_{B1\text{-}9}}$ and $\mathbf{III_{E4\text{-}9}}$) were produced in lower yields and were sparingly soluble in dimethyl sulfoxide (DMSO) and other solvents, making their characterization and analysis difficult. The remaining 75 library products were subjected to purity determinations by LC-MS, NMR, and high-resolution mass spectroscopy (HRMS). Complete spectroscopic analyses using ^{1}H NMR, ^{13}C NMR, and HRMS were carried out on a random sampling of ~50% of the library (47 compounds). NMR purity determinations using hexamethyl disiloxane (HMDSO) as an internal standard were carried out on selected 10% of the library (9 samples, Table 1 and Supporting Information).

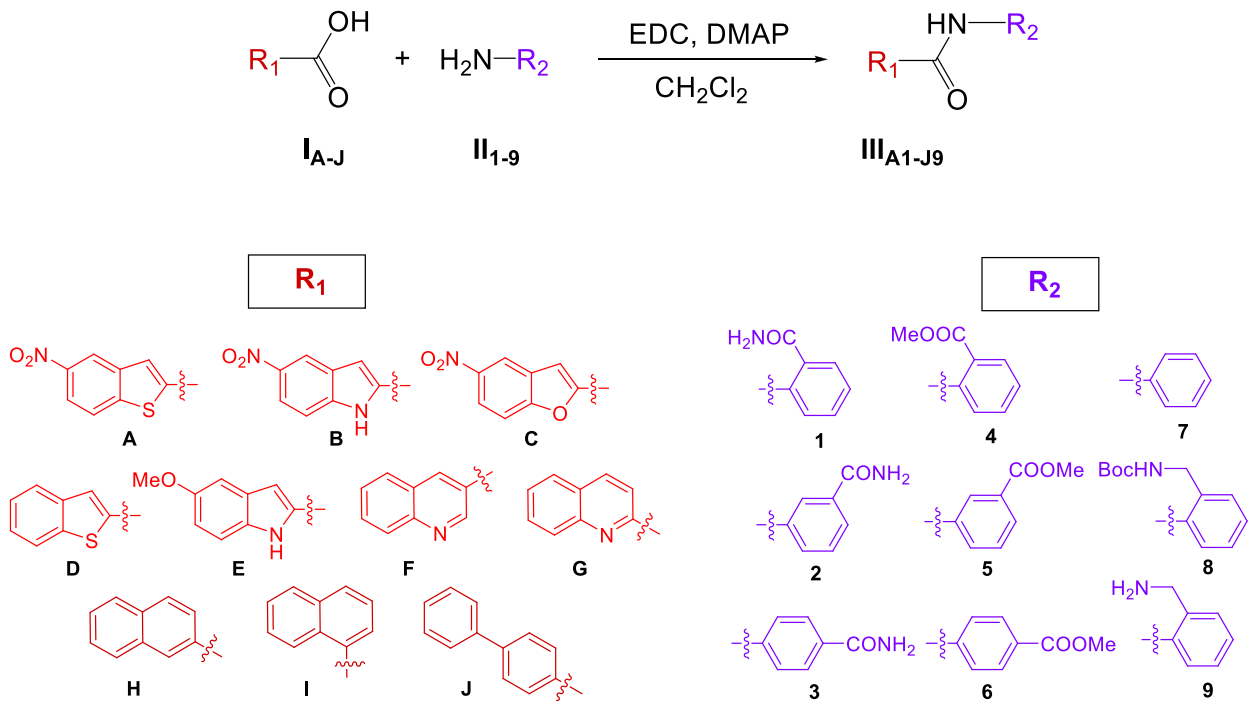

Figure 2. Synthesis of **G43** analogs.

https://dx.doi.org/10.1021/acsmedchemlett.0c00373
ACS Med. Chem. Lett. 2021, 12, 48−55

Table 1. Characterization of G43 Analogs $III_{A2\text{-}J9}$ and Their Biofilm Inhibition Profiles

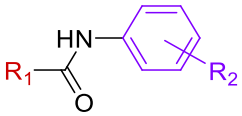

Compd No	R_1 Group	R_2 Group	LC-MS Purity (%)	Yield (%)	Solubility (μg/mL)[e]	Biofilm IC_{50} (μM)[h]
G43[a]	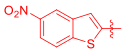	*o*-$CONH_2$	90	89	10	16.7 ± 2.3
III_{A2}[b]		*m*-$CONH_2$	93	92	25	42.3 ± 8.6
III_{A3}		*p*-$CONH_2$	100	79	*f*	>300
III_{A4}		*o*-COOMe	100	61	*f*	>300
III_{A5}[a,b]		*m*-COOMe	95	94	25	54.4 ± 9.6
III_{A6}[a,b]		*p*-COOMe	100	53	10	9.6 ± 1.1
III_{A7}[a]		H	95	91	10	>300
III_{A8}[a]		CH_2NHBoc	100	92	<5	51.5 ± 5.0
III_{A9}[a]		CH_2NH_2	80	62	1000*	106.2 ± 11.6
III_{B1}[c]	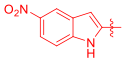	*o*-$CONH_2$	*d*	50	*g*	*d*
III_{B2}[c]		*m*-$CONH_2$	*d*	63	*g*	*d*
III_{B3}[c]		*p*-$CONH_2$	*d*	51	*g*	*d*
III_{B4}[c]		*o*-COOMe	*d*	26	*g*	*d*
III_{B5}[c]		*m*-COOMe	*d*	30	*g*	*d*
III_{B6}[c]		*p*-COOMe	*d*	28	*g*	*d*
III_{B7}[c]		H	*d*	47	*g*	*d*
III_{B8}[c]		CH_2NHBoc	*d*	64	*g*	*d*
III_{B9}[c]		CH_2NH_2	*i*	*i*	*i*	*i*
III_{C1}[a,b]	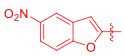	*o*-$CONH_2$	100	80	5	102.7 ± 6.4
III_{C2}[a]		*m*-$CONH_2$	100	53	20	38.8 ± 2.8
III_{C3}		*p*-$CONH_2$	71	70	*f*	>300
III_{C4}[a]		*o*-COOMe	100	78	25	71.4 ± 17.8
III_{C5}[a]		*m*-COOMe	95	86	25	2.7 ± 0.9
III_{C6}[a]		*p*-COOMe	100	66	20	144.0 ± 5.1
III_{C7}		H	66	79	25	>300
III_{C8}[a]		CH_2NHBoc	80	85	25	26.8 ± 3.9
III_{C9}		CH_2NH_2	81	79	5	98.3 ± 12.6
III_{D1}[a]		*o*-$CONH_2$	100	53	<5	45.6 ± 3.5
III_{D2}[a]		*m*-$CONH_2$	96	99	<5	115.9 ± 7.2
III_{D3}[a]		*p*-$CONH_2$	85	73	25	45.6 ± 7.1
III_{D4}		*o*-COOMe	93	62	*f*	>300
III_{D5}		*m*-COOMe	72	59	*f*	120.7 ± 13.4
III_{D6}[a]		*p*-COOMe	100	40	20	41.2 ± 8.6
III_{D7}		H	78	74	*f*	>300
III_{D8}[a]		CH_2NHBoc	88	66	20	43.4 ± 4.9
III_{D9}		CH_2NH_2	66	80	*f*	167.2 ± 14.0
III_{E1}[d]	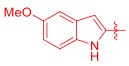	*o*-$CONH_2$	95	88	10	>300
III_{E2}[d]		*m*-$CONH_2$	94	93	5	56.6 ± 8.0
III_{E3}		*p*-$CONH_2$	97	83	*f*	>300
III_{E4}[c]		*o*-COOMe	*d*	79	*g*	*d*
III_{E5}[a]		*m*-COOMe	*d*	84	*g*	*d*
III_{E6}[c]		*p*-COOMe	*d*	86	*g*	*d*
III_{E7}		H	*d*	81	*g*	*d*
III_{E8}[c]		CH_2NHBoc	*d*	72	*g*	*d*
III_{E9}[c]		CH_2NH_2	*d*	42	*g*	*d*
III_{F1}[a,b]		*o*-$CONH_2$	100	44	5	15.3 ± 1.8
III_{F2}[a]		*m*-$CONH_2$	87	78	<5	8.6 ± 2.9
III_{F3}		*p*-$CONH_2$	98	69	*f*	>300
III_{F4}[a]		*o*-COOMe	74	88	<5	141.7 ± 3.8
III_{F5}		*m*-COOMe	87	91	*f*	147.3 ± 8.3
III_{F6}[a]		*p*-COOMe	100	49	<5	92.3 ± 3.6
III_{F7}[a]		H	100	48	5	>300
III_{F8}[a]		CH_2NHBoc	88	82	15	52.8 ± 7.9
III_{F9}		CH_2NH_2	100	83	5	135.6 ± 11.6
III_{G1}[a]		*o*-$CONH_2$	100	86	10	165.2 ± 20.4
III_{G2}[a]		*m*-$CONH_2$	100	75	10	111. 0 ± 11.7
III_{G3}[a]		*p*-$CONH_2$	100	69	5	54.4 ± 3.4
III_{G4}[a]		*o*-COOMe	96	77	<5	89.5 ± 8.5
III_{G5}		*m*-COOMe	80	81	25	92.3 ± 10.3
III_{G6}		*p*-COOMe	63	65	25	105.6 ± 1.6
III_{G7}		H	72	70	25	>300
III_{G8}[a]		CH_2NHBoc	100	92	<5	67.5 ± 12.2
III_{G9}		CH_2NH_2	92	88	25	202.1 ± 16.8
III_{H1}[a]		*o*-$CONH_2$	98	90	25	84.1 ± 9.8
III_{H2}[a]		*m*-$CONH_2$	84	76	<5	240 ± 8.8
III_{H3}[a,b]		*p*-$CONH_2$	85	82	<5	109.7 ± 0.2
III_{H4}[a]		*o*-COOMe	98	94	25	121.3 ± 34
III_{H5}[a]		*m*-COOMe	90	85	5	>300
III_{H6}[a,b]		*p*-COOMe	84	79	25	111.7 ± 3.8
III_{H7}		H	90	69	*f*	>300
III_{H8}		CH_2NHBoc	91	75	*f*	56.8 ± 3.9
III_{H9}		CH_2NH_2	82	65	*f*	160.1 ± 8.5
III_{I1}		*o*-$CONH_2$	95	85	*f*	150.1 ± 10
III_{I2}[a]		*m*-$CONH_2$	89	92	10	195.2 ± 13.1
III_{I3}[a]		*p*-$CONH_2$	100	67	<5	167.3 ± 16.1
III_{I4}[a,b]		*o*-COOMe	85	71	5	>300
III_{I5}		*m*-COOMe	72	80	<5	>300
III_{I6}		*p*-COOMe	90	78	*f*	>300
III_{I7}		H	81	86	*f*	>300
III_{I8}[a]		CH_2NHBoc	83	98	5	195.6 ± 9
III_{I9}[a]		CH_2NH_2	99	80	25	224.3 ±17
III_{J1}[a]	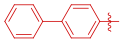	*o*-$CONH_2$	100	76	5	193.3 ± 7.9
III_{J2}[a]		*m*-$CONH_2$	98	81	25	79.9 ± 4.2
III_{J3}[a]		*p*-$CONH_2$	100	89	<5	>300
III_{J4}		*o*-COOMe	78	95	*f*	>300
III_{J5}[a,b]		*m*-COOMe	89	78	<5	105.1 ± 0.4
III_{J6}[a]		*p*-COOMe	86	71	*f*	>300
III_{J7}		H	60	89	*f*	>300
III_{J8}[a]		CH_2NHBoc	97	82	<5	123.8 ± 8.1
III_{J9}		CH_2NH_2	91	91	*f*	195.6 ± 9

[a]Fully characterized with ^1H NMR, ^{13}C NMR, and HRMS. [b]Purity determined to be above 90% by ^1H NMR internal standard measurements using HMDSO as standard. [c]Unable to characterize due to poor solubility. [d]Unable to collect data due to poor solubility. [e]Solubility in water. [f]Not determined. [g]Insoluble. [h]Values represent the means ± standard deviations from three independent experiments. [i]Reaction did not work. *TFA salt.

The structural modifications of **G43** were guided by its docking model within the GtfC active site generated using FlexX/LeadIT (Figure 3).[24,25] According to this model **G43** occupies the same space as the ligand (acarbose) in the reported X-ray crystal structure and is within the H-bonding distance from the three critical active site catalytic residues, Glu515, Asp477, and Asp588.[26] The ortho amide group of **G43** that is critical for its activity was found to be making direct H-bonding interactions with two of these residues, Glu515 and Asp477 (Figure 3).

We chose to incorporate different bicyclic ring systems in the place of the benzothiophene ring (left) and different substituents on the phenyl ring (right) of **G43** using a combination of both rational and classical medicinal chemistry approaches. For example, the primary amide group on the phenyl ring of **G43** holds protons weakly. Amines, on the other hand, are strong proton acceptors due to the higher availability of the lone pair of electrons on the nitrogen atom to accept acidic hydrogens. This small manipulation in compound $\mathbf{III_{A9}}$ improves the predicted binding energy from −32 to −39 kJ/mol (Figure 4). This change in the functional group from amide to amine group improved the interactions with Asp588 due to the increase in rotation and flexibility gained from the change in hybridization of the amide carbon atom from sp^2 to sp^3, contributing to the overall improved score.

The S atom within the left ring of **G43** is predicted to have no specific interactions with any of the active site residues. Changing the S to NH in compound $\mathbf{III_{B1}}$ resulted in the binding of the newly added NH with the negatively charged Asp909 in the proximity (Figure 4). This modification also altered the bond angles within the lead molecule, which produces additional interactions as reflected by the improved binding energy of −37 kJ/mol. This derivative also interacts with the residues Glu515 and Asp588, justifying its improved binding score. As an extension of these studies, we have conducted docking studies to explore the inclusion of bicyclic systems such as the quinoline ring as shown in compound $\mathbf{III_{F1}}$, which was able to engage all three key residues, Glu515, Asp 477, and Asp 588 and had an improved binding energy of −37 kJ/mol.

We evaluated the effects of all of the library products on *S. mutans* growth and viability to determine the selectivity toward inhibiting the biofilm versus bacterial growth. Consistent with our hypothesis, no significant difference in *S. mutans* cell viability was observed between the control group and treated groups for all library products up to 100 μM, suggesting that the compounds are not bactericidal toward *S. mutans*. Potent selective biofilm inhibitors were then analyzed with serial dilutions to determine accurate biofilm inhibition IC_{50} values (Table 1). The left side modification of **G43** resulted in a

https://dx.doi.org/10.1021/acsmedchemlett.0c00373
ACS Med. Chem. Lett. 2021, 12, 48−55

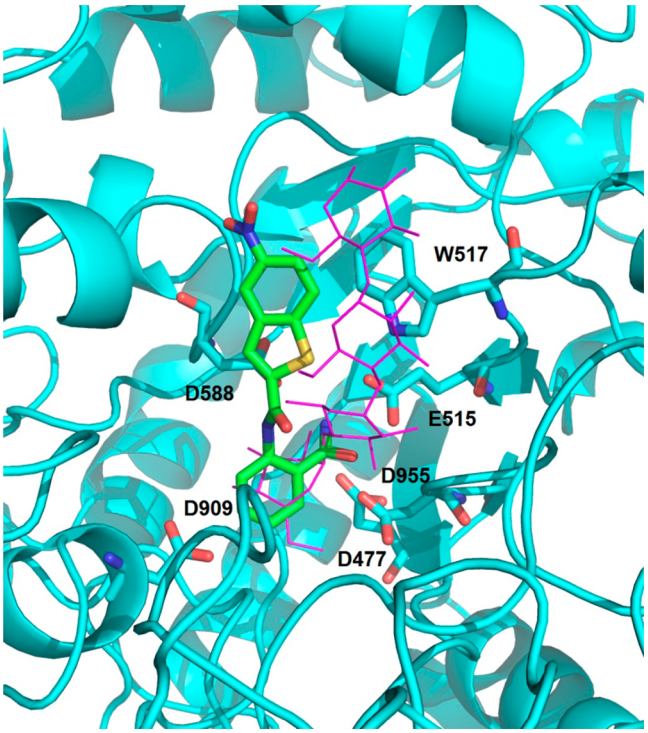

Figure 3. Docking model of **G43** (green sticks) superposed on the crystal structure of acarbose (pink line) within the GtfC catalytic site. Key active site interactions are depicted by displaying residue chains (blue sticks).

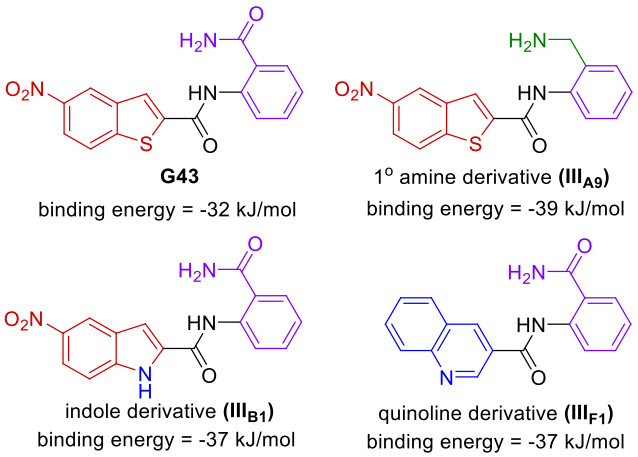

Figure 4. Chemical structures and binding energies of **G43** and a few of its derivatives.

number of biofilm inhibitors with IC_{50} values ranging from 15.3 μM to 193.3 μM with considerable variations related to specific structural modifications. For example, removal of the nitro group (**III**$_{D1}$) and substitution of the ring with naphthyl (**III**$_{H1}$ and **III**$_{I1}$) and biphenyl rings (**III**$_{J1}$) resulted in decrease in activity. The docking model predicted indole compounds to have increased interactions with the GtfC active site residues. However, the indole series were largely insoluble in DMSO and other solvents making its characterization and evaluation difficult.

The *o*-$CONH_2$ group at the right end of **G43** was modified in many ways. Its complete removal (**III**$_{A7\text{-}J7}$) resulted in total loss of activity. Changing it to the *m*-position (**III**$_{A2}$) decreased the activity, while changing it to the *p*-position (**III**$_{A3}$) nullified the activity. These observations were consistent with our docking model predicting key interactions of the *o*-$CONH_2$ group with active site residues. However, substitution of the *o*-$CONH_2$ group with *o*-COOMe groups produced a different trend. The *o*-COOMe group (**III**$_{A4}$) nullified the activity, *m*-COOMe (**III**$_{A5}$) was less active, and *p*-COOMe (**III**$_{A6}$) was more active than **G43**. The effect of replacement of *o*-$CONH_2$ with *o*-CH_2NH_2 can be seen in **III**$_{A9}$. Contrary to the prediction by the model, the IC_{50} value of **III**$_{A9}$ was 106.2 μM compared to 16.7 μM for the **G43**. Interestingly, the Boc protected intermediate (**III**$_{A8}$) was found to be more potent than the free amine counterpart (**III**$_{A9}$) with an IC_{50} value of 51.5 μM.

Several key SAR observations could be drawn for the structural modifications to either ends of **G43** from the average biofilm IC_{50} value for each series (Figure 5). While a clear trend is not apparent when comparing benzothiophene and benzofuran series, an overall trend can be deduced. The average biofilm inhibitory activity is comparable, exhibiting 131 μM and 121 μM for benzothiophene (**III**$_{A1\text{-}9}$) and benzofuran (**III**$_{C1\text{-}9}$) series, respectively. The indolyl (**III**$_{B1\text{-}9}$) and 2-quinolinyl (**III**$_{G1\text{-}9}$) series of compounds offer a comparison of the ring size and its effect on the biofilm inhibition. As previously mentioned the indole series were insoluble. While the evaluated indole derivatives had no effect on the biofilm, the 2-quinolinyl derivatives exhibited micromolar inhibition, with the average IC_{50} being 132 μM. The attachment point of the left aromatic ring and its effect on activity can be observed in the 3-quinolinyl (**III**$_{F1\text{-}9}$) and 2-quinolinyl (**III**$_{G1\text{-}9}$) series, where the substituent comes off the 3-position and 2-position, respectively, and the β-naphthalene (**III**$_{H1\text{-}9}$) and α-naphthalene (**III**$_{I1\text{-}9}$) series, where the substituent comes off the 2-position and 1-position, respectively. With the exception of **III**$_{G3}$, **III**$_{G4}$, and **III**$_{G5}$ the 2-quinolines were less potent than their 3-quinoline counterparts. Similarly, the α-naphthalene (**III**$_{I1\text{-}9}$) series were less potent compared to the β-naphthalene (**III**$_{H1\text{-}9}$) series.

When the *o*-$CONH_2$ group was removed in the **III**$_{A7\text{-}J7}$ series, to have an unsubstituted benzene ring on the right side, the activity was nullified in all examples up to 300 μM, highlighting the importance of the *o*-$CONH_2$ group. The overall trends in average IC_{50} values revealed that the primary amide regiochemistry is also crucial for the activity of the compound. Compared to the *o*-position, the placement of this functional group in the *m*-position marginally increased potency. The 3-quinolinyl analog **III**$_{F2}$ in particular had an improved IC_{50} value of 8.6 μM. On the other hand, the *p*-$CONH_2$ group almost consistently reduced the activity with the exception of **III**$_{D3}$, **III**$_{G3}$, and **III**$_{H3}$. The primary amide group was replaced with a methyl ester functionality in series **III**$_{4\text{-}6}$. Interestingly, this moiety at the *o*-position did not serve to increase the potency and in several instances nullified the activity of the compounds, as seen in **III**$_{A4}$, **III**$_{D4}$, **III**$_{H4}$, and **III**$_{J4}$. Remarkably, this functional group in the *m*- and *p*-positions was able to give the right combination of interactions to elevate the potency. For example, the compound **III**$_{C5}$, a 5-nitrobenzofuran derivative with an *m*-COOMe group, produced the best IC_{50} value of 2.7 μM, making it the most potent compound identified from this library. Through the SAR studies, we have identified several new analogs that are either equally or more potent than **G43** (Figure 6A). Docking models of these compounds indicated that their binding modes

https://dx.doi.org/10.1021/acsmedchemlett.0c00373
ACS Med. Chem. Lett. 2021, 12, 48−55

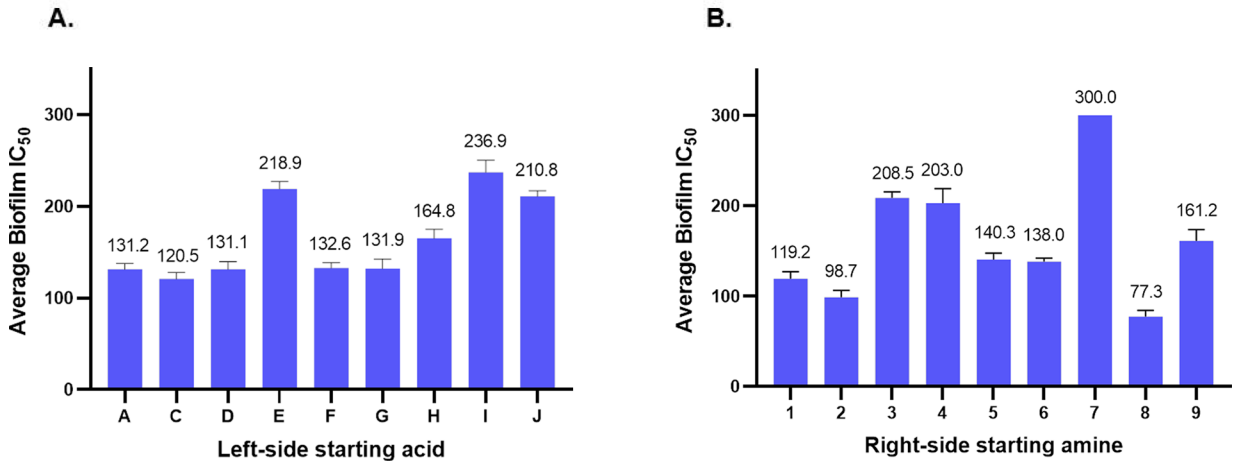

Figure 5. (A) Average biofilm IC_{50} values for varying left-side modifications. (B) Average biofilm IC_{50} values for varying right-side modifications. The highest tested concentration of 300 μM is used for the average IC_{50} calculations of the inactive compounds.

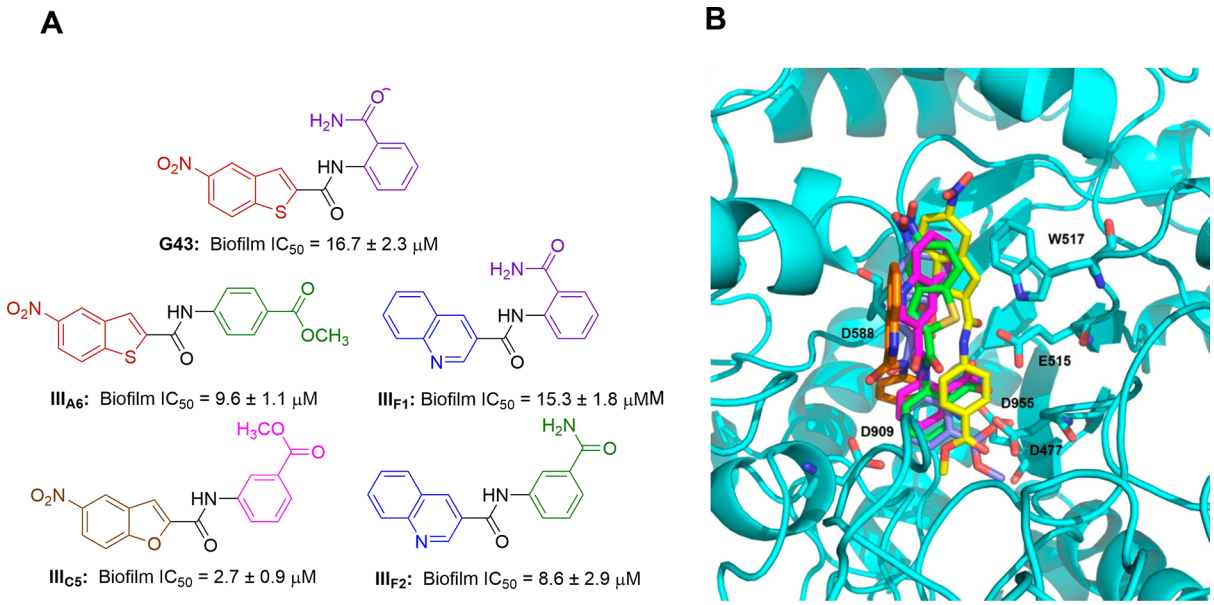

Figure 6. (A) Chemical structures of **G43** and its more active analogs identified from the SAR studies. (B) Docking models of $\mathbf{III_{A6}}$ (yellow), $\mathbf{III_{F1}}$ (magenta), $\mathbf{III_{C5}}$ (violet), and $\mathbf{III_{F2}}$ (gold) in the GtfC active site compared with **G43** (green).

are quite similar to what we have observed for **G43** with the exception of $\mathbf{III_{F2}}$, which took a slightly different binding mode. Compounds $\mathbf{III_{A6}}$, $\mathbf{III_{F1}}$, and $\mathbf{III_{C5}}$ engaged at least two of the three catalytic site residues while $\mathbf{III_{F2}}$ was shown to engage all three residues (Figure 6B).

It is important to note that although *in-silico* screening and docking studies were performed against GtfC, significant inhibition of both GtfB and GtfC is expected for our inhibitors as both these targets have a very similar amino acid composition (93.61% sequence identity), both are subject to the same regulatory processes, and the genes encoding GtfB and GtfC lie close to each other.[27] The structural similarity between GtfB and GtfC is shown in the overlay of the homology model of chain A of GtfB on the crystal structure of chain A of GtfC (Figure 7A) and almost indentical binding modes of **G43** in the active sites of GtfB and GtfC (Figure 7B).

We have subjected several of our key compounds to a reported zymogram assay[28] that offers a qualitative observation of the inhibition of Gtfs through the intensity of the glucan bands produced. As seen in Figure 8A, there was a definite decrease in the production of glucans synthesized by GtfC, the bottom band. There was also a decrease in the upper band in which GtfB and GtfD remain unseparated, suggesting that the compounds act upon at least two, if not all three Gtfs. Compounds $\mathbf{III_{A6}}$, $\mathbf{III_{A8}}$, $\mathbf{III_{F1}}$, $\mathbf{III_{F2}}$, and $\mathbf{III_{F8}}$ along with two control compounds **G43** and **G16**,[23] showed a higher potency in the biofilm assay and also appeared to be more potent in the zymogram assay. These results suggest that the inhibitory effect seen on the *S. mutans* biofilms is through the inhibition of *S. mutans* Gtfs.

Based on the SAR studies and the zymogram results, we selected compound $\mathbf{III_{F1}}$ for further evaluation in an animal model of dental caries. This selection was based on its potency, selectivity, novelty of the chemical structure, and potential for future preclinical development. Other optimized compounds such as $\mathbf{III_{C5}}$ or $\mathbf{III_{A6}}$ with better biofilm inhibition were not pursued due to the presence of the undesirable NO_2 group in their structure. Prior to the animal studies, the bactericidal

https://dx.doi.org/10.1021/acsmedchemlett.0c00373
ACS Med. Chem. Lett. 2021, 12, 48−55

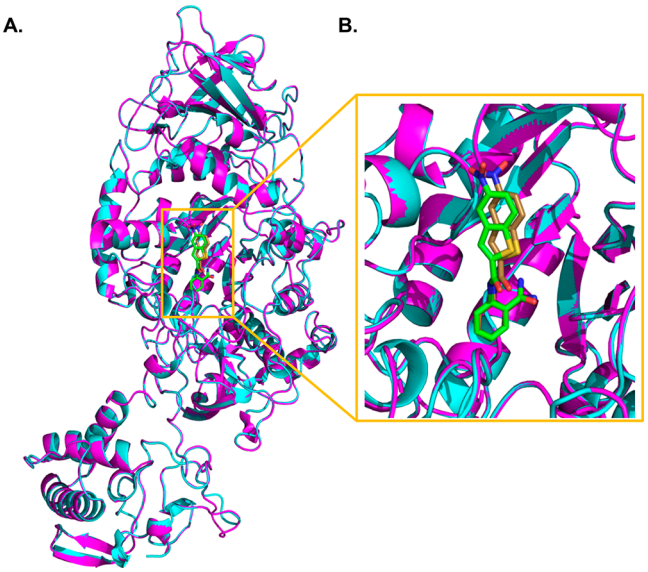

Figure 7. (A) Overlay of the homology model of the GtfB chain A (magenta) with the crystal structure of the GtfC chain A (blue) with **G43** bound. (B) Binding modes of **G43** in the active site of GtfB (gold sticks) compared with GtfC (green sticks).

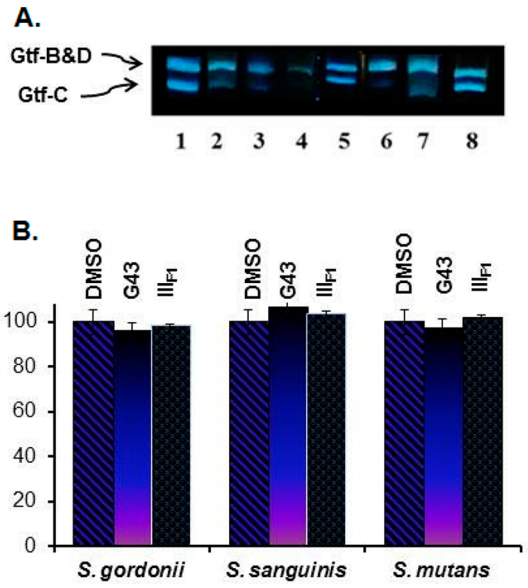

Figure 8. (A) Effects of selected compounds on the activity of Gtfs by zymographic assays, lane-1: DMSO, lane-2: **G43**, lane-3: **G16**, lane-4: $\mathbf{III_{A6}}$, lane-5: $\mathbf{III_{A8}}$, lane-6: $\mathbf{III_{F1}}$, lane-7: $\mathbf{III_{F2}}$, and lane-8: $\mathbf{III_{F8}}$. Zymographic assays were performed using SDS-PAGE analysis of Gtfs from culture supernatants of *S. mutans* UA159 incubated with vehicle control DMSO, the compounds 50 μM. (B) Effects of **G43** or $\mathbf{III_{F1}}$ on commensal species. *S. gordonii*, *S. sanguinis*, and *S. mutans* were treated with 100 μM of the compound or DMSO and bacterial growth was measured at OD470 and normalized to the DMSO control (100%). The p value is $\leq$0.05.

activities of $\mathbf{III_{F1}}$ and the control compound **G43** were further investigated to rule out the possibility that observed biofilm inhibition is a result of bactericidal activity and to confirm that they do not affect the growth of oral commensals. Both compounds were evaluated against representative commensal oral bacteria, *S. sanguinis* and *S. gordonii*, along with *S. mutans*, and demonstrated that they do not affect the growth at 100 μM (Figure 8B).

The effect of compound $\mathbf{III_{F1}}$ on *S. mutans* colonization and virulence was evaluated using a rat model of dental caries (Figure 9).[29] Compound **G43** was included in these studies for

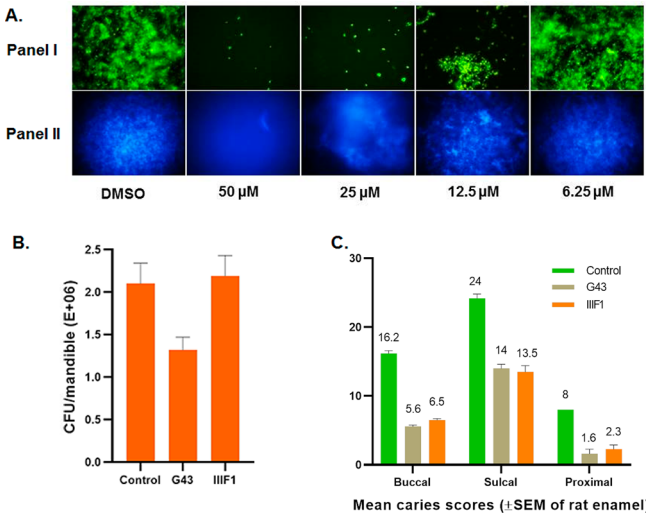

Figure 9. (A) Fluorescent microscopy images of *S. mutans* UA159 biofilms with its treatment with serial dilutions of $\mathbf{III_{F1}}$. Panel I: Viable bacterial cells within biofilm were stained with 2.5 μM Syto9 (green). Panel II: Dextran-conjugated cascade blue labeled exopolysaccharides within *S. mutans* biofilm. (B) Effect of treatment with **G43** or $\mathbf{III_{F1}}$ on the susceptibility of gnotobiotic rats to *S. mutans* UA159 infection and dental caries activity. Rats infected starting at 22 days of age and placed on Diet 305. Rats were sacrificed at 64 days of age (day 43). No significant differences in the body weights of treated and untreated rats. No significant difference in CFU/mL for $\mathbf{III_{F1}}$ treated and untreated rats. (C) Caries Scores: buccal and proximal: $p < 0.00$, sulcal: $p < 0.001$. Significant reduction in buccal, sulcal, and proximal caries scores was observed in animals treated with **G43** or $\mathbf{III_{F1}}$.

comparison. The biofilm inhibition profile of $\mathbf{III_{F1}}$ is presented in Figure 9A. All rats from the two experimental groups and from the control (vehicle + infection only) group were colonized with *S. mutans*. The bacterial colonization appears to be reduced in **G43** treated rats when compared with the control group while the novel analog, $\mathbf{III_{F1}}$ had no effect on the bacterial colonization, suggesting that it is less toxic to bacteria than **G43** (Figure 9B). The buccal, sulcal, and proximal surface caries scores of the treated animals were significantly reduced in both cases (Figure 9C). These data suggest that both compounds selectively target virulence factors and Gtfs and Gtf- mediated biofilm formation, rather than a simple inhibition of bacterial growth. Furthermore, as observed with **G43**,[23] rats treated with $\mathbf{III_{F1}}$ did not exhibit any weight loss over the course of the study in comparison with the control group, suggesting that the compounds are nontoxic to animals.

In conclusion, Gtfs are indispensable virulence factors for the cariogenesis of *S. mutans*. We have synthesized a library of 90 derivatives of **G43** to study the SAR and have uncovered several crucial groups and their respective regiochemistry needed for potent biofilm inhibition. We have identified several new analogs that are either equally or more potent than **G43**. The most active compound, $\mathbf{III_{C5}}$ inhibited *S. mutans* biofilm with an IC_{50} value of 2.7 μM. Selected compounds from this library were further evaluated for enzyme inhibition against Gtfs using a zymogram assay and for growth inhibition against

https://dx.doi.org/10.1021/acsmedchemlett.0c00373
ACS Med. Chem. Lett. 2021, 12, 48−55

oral commensal bacterial species. This study has led to the discovery of several new biofilm inhibitors with enhanced potency and selectivity. One of the lead compounds, $\mathbf{III_{F1}}$, showed marked reduction in buccal, sulcal, and proximal caries scores in a rat model of dental caries.

■ ASSOCIATED CONTENT

Supporting Information

The Supporting Information is available free of charge at https://pubs.acs.org/doi/10.1021/acsmedchemlett.0c00373.

Spectral characterization, spectra, synthetic procedures, and biological protocols (PDF)

■ AUTHOR INFORMATION

Corresponding Authors

Sadanandan E. Velu − *Department of Chemistry, University of Alabama at Birmingham, Birmingham, Alabama 35294, United States*; orcid.org/0000-0002-0342-2378; Phone: (503) 418-2090; Email: wuhu@ohsu.edu

Hui Wu − *Department of Integrative Biomedical and Diagnostic Sciences, Oregon Health and Science University, Portland, Oregon 97239, United States*; Phone: (205) 975-2475; Email: svelu@uab.edu

Authors

Bhavitavya Nijampatnam − *Department of Chemistry, University of Alabama at Birmingham, Birmingham, Alabama 35294, United States*

Parmanand Ahirwar − *Department of Chemistry, University of Alabama at Birmingham, Birmingham, Alabama 35294, United States*

Piyasuda Pukkanasut − *Department of Chemistry, University of Alabama at Birmingham, Birmingham, Alabama 35294, United States*

Holly Womack − *Department of Chemistry, University of Alabama at Birmingham, Birmingham, Alabama 35294, United States*

Luke Casals − *Department of Chemistry, University of Alabama at Birmingham, Birmingham, Alabama 35294, United States*

Hua Zhang − *Department of Pathology, University of Alabama at Birmingham, Birmingham, Alabama 35294, United States*

Xia Cai − *Department of Microbiology, University of Alabama at Birmingham, Birmingham, Alabama 35294, United States*

Suzanne M. Michalek − *Department of Microbiology, University of Alabama at Birmingham, Birmingham, Alabama 35294, United States*

Complete contact information is available at: https://pubs.acs.org/10.1021/acsmedchemlett.0c00373

Author Contributions

[⊥]B.N. and P.A. contributed equally to this manuscript. Conceived the idea and designed the experiments: S.E.V., H.Wu, and S.M.; Performed the experiments: B.N., P.A., P.P., and H.W., L.C., H.Z., and X.C. Drafted and finalized the manuscript, B.N., S.E.V., and H.Wu.

Notes

The authors declare no competing financial interest.

■ ACKNOWLEDGMENTS

This study was funded by the National Institute of Dental and Craniofacial Research, National Institutes of Health grants R21DE028349 and R03DE025058 to Velu, R01DE022350 to Wu, and F31DE025783 to Nijampatnam.

■ ABBREVIATIONS

Gtf, glucosyltransferases; *S. mutans*, *Streptococcus mutans*; *S. sanguinis*, *Streptococcus sanguinis*; *S. gordonii*, *Streptococcus gordonii*; SAR, structure activity relationship; EDC, *N*-ethyl-*N*′-(3-dimethylaminopropyl)carbodiimide; DMAP, *N*,*N*-dimethyl aminopyridine; TFA, trifluoroacetic acid; DMSO, dimethyl sulfoxide; HRMS, high resolution mass spectrometry; LC-MS, liquid-chromatography mass spectrometry; NMR, nuclear magnetic resonance; HMDSO, hexamethyl disiloxane; BOC, *tert*-butyloxy carbonyl; IC_{50}, half maximal inhibitory concentration; SDS-PAGE, sodium dodecyl sulfate-polyacrylamide gel electrophoresis; CFU, colony forming unit

■ REFERENCES

(1) Marsh, P. D. Dental plaque as a microbial biofilm. *Caries Res.* **2004**, *38* (3), 204−11.

(2) Hamada, S.; Slade, H. D. Biology, immunology, and cariogenicity of Streptococcus mutans. *Microbiol. Rev.* **1980**, *44* (2), 331−84.

(3) Loesche, W. J. Role of Streptococcus mutans in human dental decay. *Microbiol. Rev.* **1986**, *50* (4), 353−80.

(4) Bowden, G. H.; Hamilton, I. R. Survival of oral bacteria. *Crit. Rev. Oral Biol. Med.* an official publication of the American Association of Oral Biologists **1998**, *9* (1), 54−85.

(5) Kim, D.; Barraza, J. P.; Arthur, R. A.; Hara, A.; Lewis, K.; Liu, Y.; Scisci, E. L.; Hajishengallis, E.; Whiteley, M.; Koo, H. Spatial mapping of polymicrobial communities reveals a precise biogeography associated with human dental caries. *Proc. Natl. Acad. Sci. U. S. A.* **2020**, *117* (22), 12375−86.

(6) Quivey, R. G., Jr.; Kuhnert, W. L.; Hahn, K. Adaptation of oral streptococci to low pH. *Adv. Microb. Physiol.* **2000**, *42*, 239−74.

(7) Chia, J. S.; Hsu, T. Y.; Teng, L. J.; Chen, J. Y.; Hahn, L. J.; Yang, C. S. Glucosyltransferase gene polymorphism among Streptococcus mutans strains. *Infect. Immun.* **1991**, *59* (5), 1656−60.

(8) Hanada, N.; Kuramitsu, H. K. Isolation and characterization of the Streptococcus mutans gtfC gene, coding for synthesis of both soluble and insoluble glucans. *Infect. Immun.* **1988**, *56* (8), 1999−2005.

(9) Hanada, N.; Kuramitsu, H. K. Isolation and characterization of the Streptococcus mutans gtfD gene, coding for primer-dependent soluble glucan synthesis. *Infect. Immun.* **1989**, *57* (7), 2079−85.

(10) Koo, H.; Xiao, J.; Klein, M. I.; Jeon, J. G. Exopolysaccharides produced by Streptococcus mutans glucosyltransferases modulate the establishment of microcolonies within multispecies biofilms. *J. Bacteriol.* **2010**, *192* (12), 3024−32.

(11) Oyanagi, T.; Tagami, J.; Matin, K. Potentials of mouthwashes in disinfecting cariogenic bacteria and biofilms leading to inhibition of caries. *Open Dent. J.* **2012**, *6*, 23−30.

(12) Kapil, V.; Haydar, S. M.; Pearl, V.; Lundberg, J. O.; Weitzberg, E.; Ahluwalia, A. Physiological role for nitrate-reducing oral bacteria in blood pressure control. *Free Radical Biol. Med.* **2013**, *55*, 93−100.

(13) Jansson, L.; Lavstedt, S.; Frithiof, L. Relationship between oral health and mortality rate. *J. Clin. Periodontol.* **2002**, *29* (11), 1029−34.

(14) Hada, L. S.; Kakiuchi, N.; Hattori, M.; Namba, T. Identification of antibacterial principles against Streptococcus mutans and inhibitory principles against glucosyltransferase from the seed of Areca catechu L. *Phytother. Res.* **1989**, *3* (4), 140−44.

(15) Nakano, Y. J.; Kuramitsu, H. K. Mechanism of Streptococcus mutans glucosyltransferases: hybrid-enzyme analysis. *J. Bacteriol.* **1992**, *174* (17), 5639−46.

(16) Yamashita, Y.; Bowen, W. H.; Burne, R. A.; Kuramitsu, H. K. Role of the Streptococcus mutans gtf genes in caries induction in the specific-pathogen-free rat model. *Infect. Immun.* **1993**, *61* (9), 3811−17.
(17) Duarte, S.; Gregoire, S.; Singh, A. P.; Vorsa, N.; Schaich, K.; Bowen, W. H.; Koo, H. Inhibitory effects of cranberry polyphenols on formation and acidogenicity of Streptococcus mutans biofilms. *FEMS Microbiol. Lett.* **2006**, *257* (1), 50−56.
(18) Ferrazzano, G. F.; Amato, I.; Ingenito, A.; De Natale, A.; Pollio, A. Anti-cariogenic effects of polyphenols from plant stimulant beverages (cocoa, coffee, tea). *Fitoterapia* **2009**, *80* (5), 255−62.
(19) Nijampatnam, B.; Casals, L.; Zheng, R.; Wu, H.; Velu, S. E. Hydroxychalcone inhibitors of Streptococcus mutans glucosyl transferases and biofilms as potential anticaries agents. *Bioorg. Med. Chem. Lett.* **2016**, *26* (15), 3508−13.
(20) Nijampatnam, B.; Zhang, H.; Cai, X.; Michalek, S. M.; Wu, H.; Velu, S. E. Inhibition of Streptococcus mutans Biofilms by the Natural Stilbene Piceatannol Through the Inhibition of Glucosyltransferases. *ACS Omega* **2018**, *3* (7), 8378−85.
(21) Newbrun, E.; Hoover, C. I.; Walker, G. J. Inhibition by acarbose, nojirimycin and 1-deoxynojirimycin of glucosyltransferase produced by oral streptococci. *Arch. Oral Biol.* **1983**, *28* (6), 531−36.
(22) Ren, Z.; Cui, T.; Zeng, J.; Chen, L.; Zhang, W.; Xu, X.; Cheng, L.; Li, M.; Li, J.; Zhou, X.; Li, Y. Molecule Targeting Glucosyltransferase Inhibits Streptococcus mutans Biofilm Formation and Virulence. *Antimicrob. Agents Chemother.* **2016**, *60* (1), 126−35.
(23) Zhang, Q.; Nijampatnam, B.; Hua, Z.; Nguyen, T.; Zou, J.; Cai, X.; Michalek, S. M.; Velu, S. E.; Wu, H. Structure-Based Discovery of Small Molecule Inhibitors of Cariogenic Virulence. *Sci. Rep.* **2017**, *7* (1), 5974.
(24) Schneider, N.; Hindle, S.; Lange, G.; Klein, R.; Albrecht, J.; Briem, H.; Beyer, K.; Claussen, H.; Gastreich, M.; Lemmen, C.; Rarey, M. Substantial improvements in large-scale redocking and screening using the novel HYDE scoring function. *J. Comput.-Aided Mol. Des.* **2012**, *26* (6), 701−23.
(25) Schneider, N.; Lange, G.; Hindle, S.; Klein, R.; Rarey, M. A consistent description of HYdrogen bond and DEhydration energies in protein-ligand complexes: methods behind the HYDE scoring function. *J. Comput.-Aided Mol. Des.* **2013**, *27* (1), 15−29.
(26) Ito, K.; Ito, S.; Shimamura, T.; Weyand, S.; Kawarasaki, Y.; Misaka, T.; Abe, K.; Kobayashi, T.; Cameron, A. D.; Iwata, S. Crystal structure of glucansucrase from the dental caries pathogen Streptococcus mutans. *J. Mol. Biol.* **2011**, *408* (2), 177−86.
(27) Hamada, S.; Horikoshi, T.; Minami, T.; Kawabata, S.; Hiraoka, J.; Fujiwara, T.; Ooshima, T. Oral passive immunization against dental caries in rats by use of hen egg yolk antibodies specific for cell-associated glucosyltransferase of Streptococcus mutans. *Infect. Immun.* **1991**, *59* (11), 4161−67.
(28) Mattos-Graner, R. O.; Napimoga, M. H.; Fukushima, K.; Duncan, M. J.; Smith, D. J. Comparative analysis of Gtf isozyme production and diversity in isolates of Streptococcus mutans with different biofilm growth phenotypes. *Journal of clinical microbiology* **2004**, *42* (10), 4586−92.
(29) Michalek, S. M.; McGhee, J. R.; Shiota, T.; Devenyns, D. Virulence of Streptococcus mutans: cariogenicity of S. mutans in adult gnotobiotic rats. *Infect. Immun.* **1977**, *15* (2), 466−71.

https://dx.doi.org/10.1021/acsmedchemlett.0c00373
ACS Med. Chem. Lett. 2021, 12, 48−55